Chapter 1

Introduction : mesoscopic physics

1.1 Interference and disorder

Wave propagation in a random medium is a phenomenon common to many areas of physics. There has been a recent resurgence of interest following the discovery, both in optics and quantum mechanics, of surprising coherent effects in a regime in which disorder was thought to be sufficiently strong to eliminate *a priori* all interference effects.

To understand the origin of these coherent effects, it may be useful to recall some general facts about interferences. Although quite spectacular in quantum mechanics, their description is more intuitive in the context of physical optics. For this reason, we begin with a discussion of interference effects in optics.

Consider a monochromatic wave scattered by an obstacle of some given geometry, *e.g.,* a circular aperture. Figure 1.1 shows the diffraction pattern on a screen placed infinitely far from the obstacle. It exhibits a set of concentric rings, alternatively bright and dark, resulting from constructive or destructive interferences. According to Huygens' principle, the intensity at a point on the screen may be described by replacing the aperture by an ensemble of virtual coherent point sources and considering the difference in optical paths associated with these sources. In this way, it is possible to associate each interference ring with an integer (the equivalent of a quantum number in quantum mechanics).

Let us consider the robustness of this diffraction pattern. If we illuminate the obstacle by an incoherent source for which the length of the emitted wave trains is sufficiently short so that the different virtual sources are out of phase, then the interference pattern on the screen will disappear and the screen will be uniformly illuminated. Contrast this with the following situation : employ a coherent light source and rapidly move the obstacle in its plane in a random fashion. Here too, the interference fringes are replaced by a uniform illumination. In this case, it is the persistence of the observer's retina that averages over many different displaced diffraction patterns. This example illustrates two
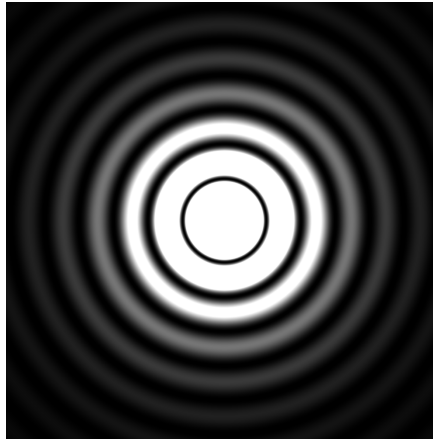
Figure 1.1: *Diffraction pattern at infinity for a circular aperture.*

ways in which the diffraction pattern can disappear. In the former case, the disappearance is associated with a random distribution of the lengths of wave trains emanating from the source, while in the latter case, it is the result of an *average* over an ensemble of spatially distributed virtual sources. This example shows how interference effects may vanish upon averaging.

Let us now turn to the diffraction of a coherent source by an obstacle of arbitrary type. For instance, suppose that the obstacle is a dielectric material whose refractive index fluctuates in space on a scale comparable to the wavelength of the light. The resulting scattering pattern, on a screen placed at infinity, consists of a random distribution of bright and dark areas, as seen in Figure 1.2; this is called a *speckle* pattern [1]. Each speckle associated with the scattering represents a *"fingerprint"* of the random obstacle, and is specific to it. However, in contrast to the case of scattering by a sufficiently symmetric obstacle (such as a simple circular aperture), it is impossible to identify an order in the speckle pattern, and thus we cannot describe it with a deterministic sequence of integer numbers. This impossibility is one of the characteristics of what are termed complex media.

In this last experiment, for a thin enough obstacle, a wave scatters only once in the random medium before it emerges on its way to the screen at infinity (see Figure 1.3.*a*). This regime is called *single scattering*. Consider now the opposite limit of an optically thick medium (also called a turbid medium), in which the wave scatters many times before leaving (Figure 1.3.*b*). We thus speak of *multiple scattering*. The intensity at a point on the screen is obtained from the sum of the complex amplitudes of the waves arriving at that point. The phase associated with each amplitude is proportional to the path length of the multiply scattered wave divided by its wavelength λ. The path lengths are

---

[1]These speckles resemble those observed with light emitted by a weakly coherent laser, but they are of a different nature. Here they result from static spatial fluctuations due to the inhomogeneity of the scattering medium.
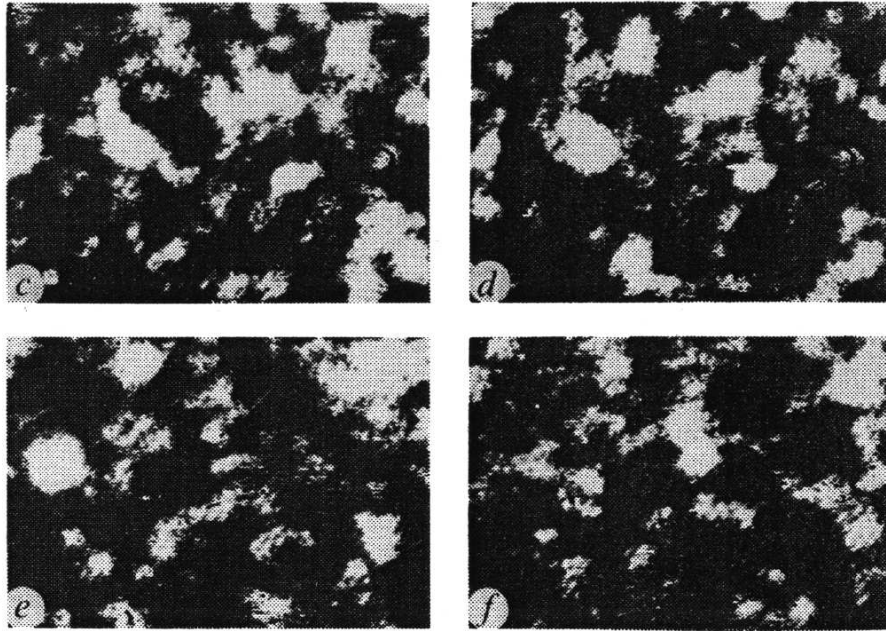
Figure 1.2: *Speckle patterns due to scattering through an inhomogeneous medium. Here the medium is optically thick, meaning that the incident radiation undergoes many scatterings before leaving the sample. Each image corresponds to a different realization of the random medium (M. Kaveh et al., Nature **326**, 778 (1987)).*

randomly distributed, so one could expect that the associated phases fluctuate and average to zero. Thus, the total intensity would reduce to the sum of the intensities associated with each of the paths.

In other words, if we represent this situation as equivalent to a series of thin obstacles, with each element of the series corresponding to a different and independent realization of the random medium, we might expect that for a sufficiently large number of such thin obstacles, the resulting intensity at a point on the screen is averaged over the different realizations, causing the speckles to vanish. This point of view corresponds to the classical description, for which the underlying wave nature plays no further role.

Figures 1.2 and 1.4 show that this conclusion is incorrect, and that the speckles survive, *even in the regime of multiple scattering.* If, on the other hand, we perform an ensemble average, the diffraction pattern disappears. This is the case with turbid media such as the atmosphere or suspensions of scatterers in a liquid (milk, for example), where the motion of the scatterers yields an average over different realizations of the random medium, provided we wait long enough. The classical approach, therefore, correctly describes the average characteristics of a turbid medium, such as the transmission coefficient or the diffusion coefficient of the average intensity. As such, it has been employed
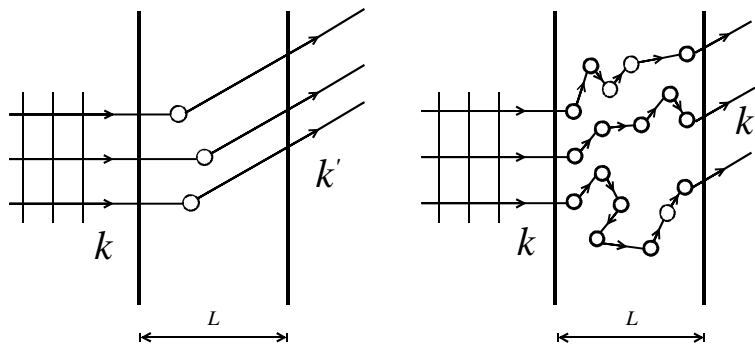
Figure 1.3: *Schematic representations of the regimes of single scattering (left), and multiple scattering (right).*

extensively in problems involving the radiative transfer of waves through the atmosphere or through turbulent media.
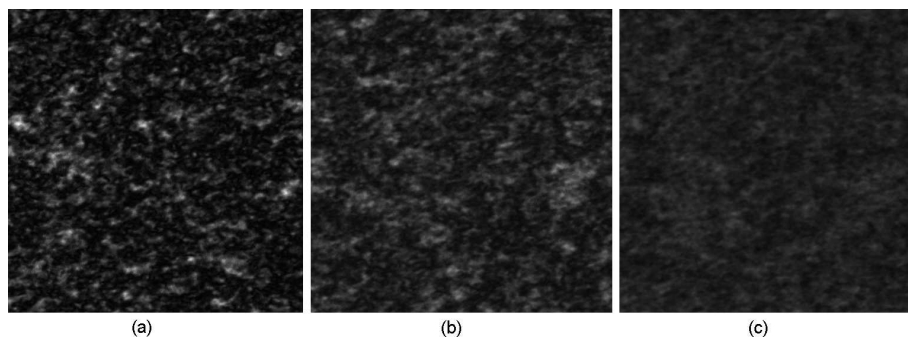

Figure 1.4: *Averaging : The first speckle pattern (a) represents a snapshot of a random medium corresponding to a single realization of the disorder. The other two figures (b and c) correspond to an integration over the motion of scatterers, and hence to a self-average. (Figure courtesy of Georg Maret).*

This description may be adapted as such to the problem of propagation of electrons in a metal. In this case, the impurities in the metal are the analog of the scatterers in the optically thick medium, and the quantity analogous to the intensity is the electrical conductivity. In principle, of course, it is necessary to use the machinery of quantum mechanics to calculate the electrical conductivity. But since the work of Drude at the beginning of the last century, it has been accepted that transport properties of metals are correctly described by the disorder-averaged conductivity, obtained from a classical description of the electron gas. However, for a given sample, *i.e.*, for a specific realization of disorder, we may observe interference effects, which only disappear upon averaging [1].

The indisputable success of the classical approach led to the belief that

coherent effects would not subsist in a random medium in which a wave undergoes multiple scattering. In the 1980s however, a series of novel experiments unequivocally proved this view to be false. In order to probe interference effects, we now turn to the Aharonov-Bohm effect, which occurs in the most spectacular of these experiments.

1.2   The Aharonov-Bohm effect

The Young two-slit device surely provides the simplest example of an interference pattern in optics; understanding its analog in the case of electrons is necessary for the understanding of quantum interference effects. In the Aharonov-Bohm geometry, an infinite solenoid is placed between the slits, such that the paths of the interfering electrons are exterior to it, as indicated in Figure 1.5. The magnetic field outside the solenoid is zero, so that classically it has no effect on the motion of the electrons.
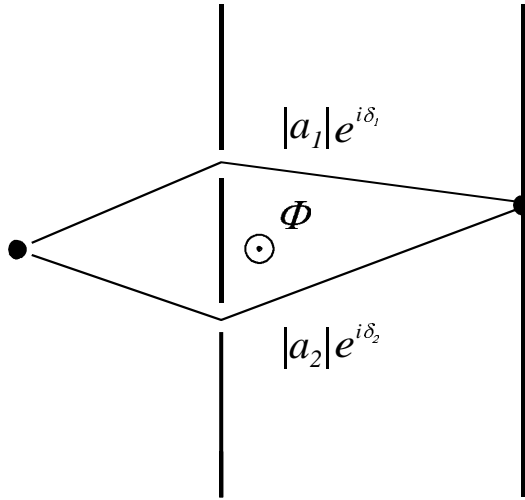

Figure 1.5: *Schematic representation of the Aharonov-Bohm effect. A flux tube of flux ϕ is placed behind the two slits.*

    This is not the case in quantum mechanics where, to calculate the intensity, we must sum the complex amplitudes associated with different trajectories. For the two trajectories of Figure 1.5, the amplitudes have the form $a_{1,2} = |a_{1,2}|e^{i\delta_{1,2}}$, where the phases δ_1 and δ_2 are given by ($-e$ is electron charge) :

$$
\begin{aligned}
\delta_1 &= \delta_1^{(0)} - \frac{e}{\hbar}\int_1 \boldsymbol{A}.d\boldsymbol{l} \\
\delta_2 &= \delta_2^{(0)} - \frac{e}{\hbar}\int_2 \boldsymbol{A}.d\boldsymbol{l} \ .
\end{aligned}
\tag{1.1}
$$

The integrals are the line integrals of the vector potential **A** along the two trajectories and $\delta_{1,2}^{(0)}$ are the phases in the absence of magnetic flux. In the

presence of a magnetic flux ϕ induced by the solenoid, the intensity $I(\phi)$ is given by

$$
\begin{aligned}
I(\phi) &= |a_1 + a_2|^2 = |a_1|^2 + |a_2|^2 + 2|a_1 a_2| \cos(\delta_1 - \delta_2) \\
&= I_1 + I_2 + 2\sqrt{I_1 I_2} \cos(\delta_1 - \delta_2) \ .
\end{aligned}
\tag{1.2}
$$

The phase difference $\Delta\delta(\phi) = \delta_1 - \delta_2$ between the two trajectories is now modulated by the magnetic flux ϕ

$$
\Delta\delta(\phi) = \delta_1^{(0)} - \delta_2^{(0)} + \frac{e}{\hbar} \oint \boldsymbol{A}.d\boldsymbol{l} = \Delta\delta^{(0)} + 2\pi \frac{\phi}{\phi_0} \ ,
\tag{1.3}
$$

where $\phi_0 = h/e$ is the quantum of magnetic flux. It is thus possible to vary continuously the state of interference at each point on the screen by changing the magnetic flux ϕ. This is the *Aharonov-Bohm effect* [2]. It is a remarkable probe to study this coherence in electronic systems [3]. This constitutes an advantage for electronic systems over their optical counterparts [2].

This effect has been observed in the following experiment : a coherent stream of electrons was emitted by an electron microscope and split in two before passing through a toroidal magnet whose magnetic field was confined to the inside of the torus [5]. Thus, the magnetic field was zero along the trajectories of electrons. This was however an experiment performed in vacuum, where the electrons do not undergo any scattering before interfering. In order to demonstrate possible phase coherence in metals, in which the electrons undergo many collisions, R. Webb and his collaborators (1983) measured the resistance of a gold ring [6]. In the setup depicted in Figure 1.6, electrons are constrained to pass through the two halves of the ring that constitute the analogs of the two Young slits, before being collected at the other end.

The analog of the intensity $I(\phi)$ is the electrical current, or better yet, the conductance $G(\phi)$ measured for different values of the magnetic flux ϕ. The flux is produced by applying a uniform magnetic field, though this does not strictly correspond to the Aharonov-Bohm experiment, since the magnetic field is not zero along the trajectories of electrons. However, the applied field is taken sufficiently weak that firstly, there is no deflection of the trajectories due to the Lorentz force, and secondly, the dephasing of coherent trajectories due to the magnetic field is negligible in the interior of the ring. Thus, the effect of the magnetic field may be neglected in comparison to that of the flux. Figure 1.7 shows that the magnetoresistance of this ring is, to first approximation, a periodic function of the applied flux whose period is the flux quantum $\phi_0 = h/e$. Indeed, since the relative phase of the two trajectories is modulated by the flux, the total current, and therefore the conductance of the ring, are periodic functions of the flux [3] :

$$
G(\phi) = G_0 + \delta G \cos(\Delta\delta^{(0)} + 2\pi \frac{\phi}{\phi_0}) \ .
\tag{1.4}
$$

---

[2]In a rotating frame, there is an analogous effect, called the Sagnac effect [4].

[3]We see in Figure 1.7 that the modulation is not purely periodic. This is due to the fact that the ring is not one-dimensional. Moreover, multiple scattering trajectories within the same branch may also be modulated by the magnetic field which penetrates into the ring itself. This is the origin of the low-frequency peak in Figure 1.7.*b*.
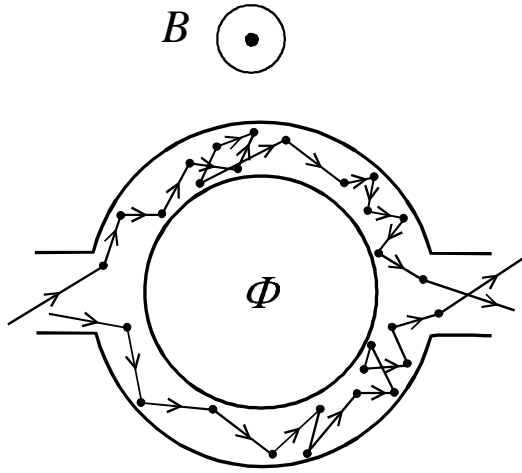
Figure 1.6: *Schematic description of the experiment of Webb et al. on the Aharonov-Bohm effect in a metal. In this experiment, the applied magnetic field is uniform. ϕ is the flux through the ring.*

This modulation of the conductance as a function of flux results from the existence of *coherent effects* in a medium in which the disorder is strong enough for electrons to be *multiply scattered*. Consequently, the naive argument that phase coherence disappears in this regime is incorrect, and must be reexamined.

1.3   Phase coherence and effect of disorder

In the aforementioned experiment of R. Webb *et al.*, the size of the ring was of the order of a micron. Now we know that for a macroscopic system, the modulation as a function of magnetic flux disappears. Therefore, there exists a characteristic length such that on scales greater than it, there is no longer any phase coherence. This length, called the *phase coherence length* and denoted L_ϕ, plays an essential role in the description of coherent effects in complex systems.

In order to better understand the nature of this length, it is useful to review some notions related to quantum coherence [4]. Consider an ensemble of quantum particles contained in a cubic box of side length L in d dimensions. The possible quantum states are coherent superpositions of wavefunctions such that the quantum state of the system is coherent over the whole volume L^d. There are many examples in which quantum coherence extends up to the macroscopic scale : superconductivity, superfluidity, free electron gas at zero temperature, coherent states of the photon field, etc.

For the electron gas at finite temperature, this coherence disappears at the macroscopic scale. It is therefore possible to treat physical phenomena such

---

[4]Most of the notions discussed here use the language of quantum mechanics; however, they have more or less direct analogs in the case of electromagnetic wave propagation.
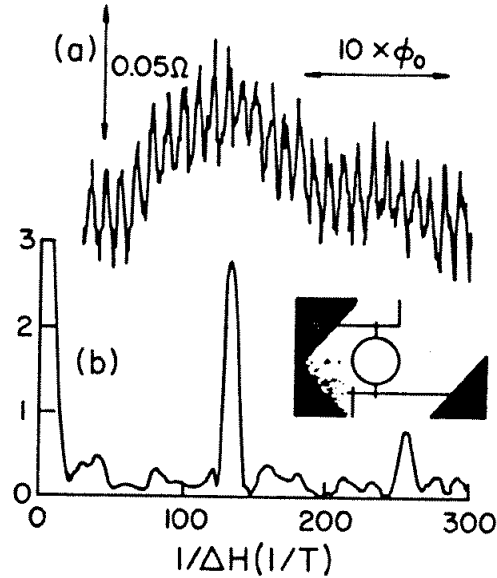
Figure 1.7: *a) Magnetoresistance of a gold ring at low temperature $T = 0.01K$, b) Fourier spectrum of the magnetoresistance. The principal contribution is that of the Fourier component at $\phi_0 = h/e$ [6].*

as electrical or thermal transport, employing an essentially classical approach. The suppression of quantum coherence results from phenomena linked to the existence of incoherent and irreversible processes due to the coupling of electrons to their environment. This environment consists of degrees of freedom with which the electrons interact : thermal excitations of the atomic lattice (phonons), impurities having internal degrees of freedom, interaction with other electrons, etc. This irreversibility is a source of decoherence for the electrons and its description is a difficult problem which we shall consider in Chapters 6 and 13. The phase coherence length L_ϕ generically describes the loss of phase coherence due to irreversible processes. In metals, the phase coherence length is a decreasing function of temperature. In practice, L_ϕ is of the order of a few microns for temperatures less than one kelvin.

None of the above considerations are related to the existence of *static* disorder of the type discussed in the two previous sections (*e.g.,* static impurities such as vacancies or substitutional disorder, or variation of the refractive index in optics). Such disorder *does not destroy the phase coherence* and does not introduce any irreversibility. However, the possible symmetries of the quantum system disappear in such a way that it is no longer possible to describe the system with quantum numbers. In consequence, each observable of a random medium depends on the specific distribution of the disordered potential. On average, it is possible to characterize the disorder by means of a characteristic length : the *elastic mean free path l_e*, which represents the average distance

travelled by a wave packet between two scattering events with no energy change (see Chapters 3 and 4).

We see, therefore, that the phase coherence length L_ϕ is fundamentally different from the elastic mean free path l_e. For sufficiently low temperatures, these two lengths may differ by several orders of magnitude, so that an electron may propagate in a disordered medium a distance much larger than l_e keeping its phase coherence, so long as the length of its trajectory does not exceed L_ϕ. The loss of coherence, therefore, is not related to the existence of a random potential of any strength, but rather to other types of mechanisms. It may seem surprising that the distinction between the effect of elastic disorder described by l_e and that associated with irreversible processes of phase relaxation was first demonstrated in the relatively nontrivial case of transport in a metal where the electrons have complex interactions with their environment. However, this same distinction also applies to electromagnetic wave propagation in turbid media in the regime of coherent multiple scattering.

1.4   Average coherence and multiple scattering

If phase coherence leads to interference effects for a specific realization of disorder, it might be thought that those would disappear upon averaging. In the experiment of R. Webb *et al.* described in section 1.2, the conductance oscillations of period $\phi_0 = h/e$ correspond to a specific ring. If we now average over disorder, that is, over $\Delta\delta^{(0)}$ in relation (1.4), we expect the modulation by the magnetic flux to disappear, and with it all trace of coherent effects. The same kind of experiment was performed in 1981 by Sharvin and Sharvin [7] on a long hollow metallic cylinder threaded by an Aharonov-Bohm flux. A cylinder of height greater than L_ϕ can be interpreted as an ensemble of identical, uncorrelated rings of the type used in R. Webb's experiment. Thus, this experiment yields an ensemble average. Remarkably, they saw a signal which still oscillates with flux but with a periodicity $\phi_0/2$ instead of ϕ_0. How can we understand that coherent effects can subsist *on average*?

The same type of question may be asked in the context of optics. If we average a speckle pattern over different realizations of disorder, does any trace of the phase coherence remain? Here too there was an unexpected result : the reflection coefficient of a wave in a turbid medium (sometimes called its albedo) was found to exhibit an angular dependence that could not be explained by the classical transport theory (Figure 1.8). This effect is known as *coherent backscattering*, and is a signature of phase coherence.

These results show that *even on average, some phase coherence effects remain.* In order to clarify the nature of these effects, let us consider an optically thick random medium. It may be modelled by an ensemble of point scatterers at positions $\boldsymbol{r}_n$ distributed randomly. The validity of this hypothesis for a realistic description of a random medium will be discussed in detail in Chapters 2 and 3. Consider a plane wave emanating from a coherent source (located outside the medium), which propagates in the medium and collides elastically with scatterers, and let us calculate the resulting interference pattern. For this, we study the complex amplitude $A(\boldsymbol{k}, \boldsymbol{k}')$ of the wave re-emitted in the direction
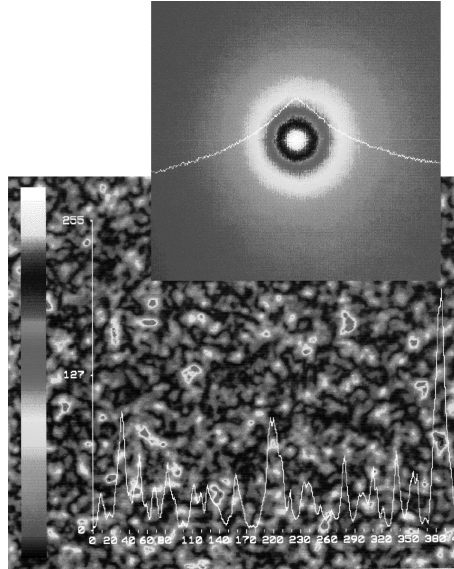
Figure 1.8: *Speckle pattern obtained by multiple scattering of light by a sample of polystyrene spheres, as a function of observation angle. The curve in the lower figure represents the intensity fluctuations measured along a given angular direction. The upper figure is obtained by averaging over the positions of the spheres, and the resulting curve gives the angular dependence of the average intensity. (Figure courtesy of G. Maret.)*

defined by the wavevector $\boldsymbol{k}'$, corresponding to an incident plane wave with wavevector $\boldsymbol{k}$. It may be written, without loss of generality, in the form

$$A(\boldsymbol{k}, \boldsymbol{k}') = \sum_{\boldsymbol{r}_1, \boldsymbol{r}_2} f(\boldsymbol{r}_1, \boldsymbol{r}_2) e^{i(\boldsymbol{k}.\boldsymbol{r}_1 - \boldsymbol{k}'.\boldsymbol{r}_2)} \quad , \tag{1.5}$$

where $f(\boldsymbol{r}_1, \boldsymbol{r}_2)$ is the complex amplitude corresponding to the propagation between two scattering events located at $\boldsymbol{r}_1$ and $\boldsymbol{r}_2$. This amplitude may be expressed as a sum of the form $\sum_j a_j = \sum_j |a_j| e^{i\delta_j}$, where each path j represents a sequence of scatterings (Figure 1.9) joining the points $\boldsymbol{r}_1$ and $\boldsymbol{r}_2$. The associated intensity is given by

$$|A(\boldsymbol{k}, \boldsymbol{k}')|^2 = \sum_{\boldsymbol{r}_1, \boldsymbol{r}_2} \sum_{\boldsymbol{r}_3, \boldsymbol{r}_4} f(\boldsymbol{r}_1, \boldsymbol{r}_2) f^*(\boldsymbol{r}_3, \boldsymbol{r}_4) e^{i(\boldsymbol{k}.\boldsymbol{r}_1 - \boldsymbol{k}'.\boldsymbol{r}_2)} e^{-i(\boldsymbol{k}.\boldsymbol{r}_3 - \boldsymbol{k}'.\boldsymbol{r}_4)} \tag{1.6}$$

with

$$f(\boldsymbol{r}_1, \boldsymbol{r}_2) f^*(\boldsymbol{r}_3, \boldsymbol{r}_4) = \sum_{j, j'} a_j(\boldsymbol{r}_1, \boldsymbol{r}_2) a_{j'}^*(\boldsymbol{r}_3, \boldsymbol{r}_4) = \sum_{j, j'} |a_j||a_{j'}| e^{i(\delta_j - \delta_{j'})} \ . \tag{1.7}$$

In order to calculate its value averaged over the realizations of the random potential, that is, over the positions of scatterers, it is useful to note that most of the terms in relations (1.6) and (1.7) average to zero, provided that the

phase $\delta_j - \delta_{j'}$, which measures the difference in the lengths of the trajectories of Figure 1.9, is random.
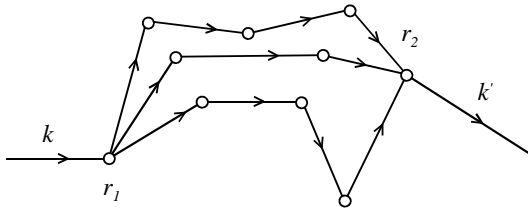

Figure 1.9: *Typical trajectories which contribute to the total complex amplitude $f(\boldsymbol{r}_1, \boldsymbol{r}_2)$ of a multiply scattered wave.*

In consequence, the only terms which contribute to the average of $|A(\boldsymbol{k}, \boldsymbol{k}')|^2$ are those for which the phases vanish. This can only occur for pairs of *identical* trajectories, those which have the same sequence of scattering events, *either in the same or in opposite directions*. Such trajectories are schematically represented in Figure 1.10, and correspond to the sequences

$$\boldsymbol{r}_1 \to \boldsymbol{r}_a \to \boldsymbol{r}_b \cdots \to \boldsymbol{r}_y \to \boldsymbol{r}_z \to \boldsymbol{r}_2$$
$$\boldsymbol{r}_2 \to \boldsymbol{r}_z \to \boldsymbol{r}_y \cdots \to \boldsymbol{r}_b \to \boldsymbol{r}_a \to \boldsymbol{r}_1$$

The fact that the trajectories are identical imposes on us, in particular, to take $\boldsymbol{r}_1 = \boldsymbol{r}_3$ and $\boldsymbol{r}_2 = \boldsymbol{r}_4$ for the former process (same direction) and $\boldsymbol{r}_1 = \boldsymbol{r}_4$ and $\boldsymbol{r}_2 = \boldsymbol{r}_3$ for the latter (opposite direction) in relation (1.6). These two processes contribute identically to the intensity provided that the system is invariant under time reversal. Moreover, the second process gives rise, according to (1.6), to an additional dephasing such that the only two non-zero contributions which remain upon averaging are :

$$\overline{|A(\boldsymbol{k}, \boldsymbol{k}')|^2} = \overline{\sum_{\boldsymbol{r}_1, \boldsymbol{r}_2} |f(\boldsymbol{r}_1, \boldsymbol{r}_2)|^2 \left[1 + e^{i(\boldsymbol{k}+\boldsymbol{k}')\cdot(\boldsymbol{r}_1-\boldsymbol{r}_2)}\right]} \quad , \tag{1.8}$$

where $\overline{\cdots}$ denotes averaging over the realizations of the random potential.

The essence of the present book is a systematic study of the consequences of the existence of these two processes, which survive upon averaging in the course of multiple scattering. The former process is well-known. It may be perfectly well understood in a purely classical treatment that does not take into account the existence of an underlying wave equation, since the phases exactly cancel out. In the study of electron transport in metals, this classical analysis is performed in the framework of the Boltzmann equation, while for electromagnetic wave propagation, the equivalent theory, called radiative transfer, was developed by Mie and Schwartzchild [8]. Both date from the beginning of the twentieth century.

The second term in relation (1.8) contains a phase factor. This last depends on the points $\boldsymbol{r}_1$ and $\boldsymbol{r}_2$, and the sum over these points in the averaging makes this term vanish in general, with two notable exceptions :
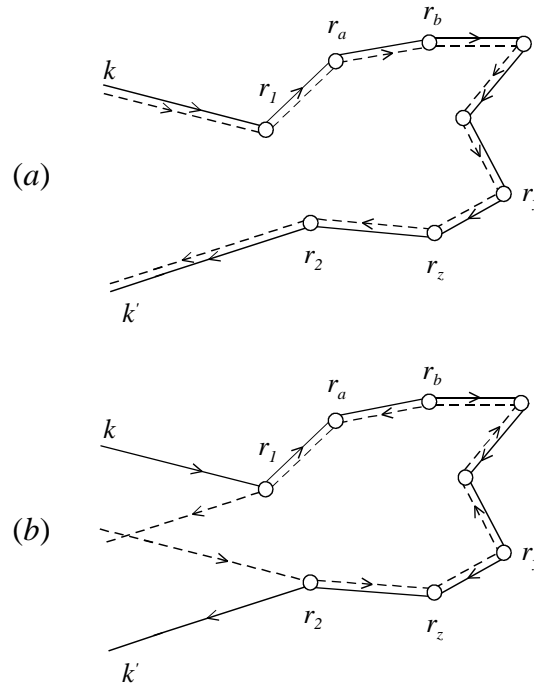
Figure 1.10: *Schematic representation of the two types of sequences of multiple scatterings that remain upon averaging. The first corresponds to the classical average intensity. The second, for which the two sequences of scattering events are traversed in opposite directions, is the source of the coherent backscattering effect.*

- $\boldsymbol{k}+\boldsymbol{k}' \simeq 0$: In the direction exactly opposite to the direction of incidence, the intensity is *twice* the classical value. The classical contribution has no angular dependence on average, and the second term, which depends on $\boldsymbol{k} + \boldsymbol{k}'$, gives an angular dependence to the average intensity reflected by the medium which appears as a peak in the albedo. This phenomenon was observed first in optics and it is known as *coherent backscattering*; its study is the object of Chapter 8.

- In the sum (1.8), the terms for which $\boldsymbol{r}_1 = \boldsymbol{r}_2$ are special. They correspond to closed multiple scattering trajectories. Their contribution to the averaged interference term survive even when it is impossible to select the directions $\boldsymbol{k}$ and $\boldsymbol{k}'$. This is the case for metals or semiconductors for which the interference term affects the average transport properties such as the electrical conductivity. This is the origin of the phenomenon of *weak localization*.

1.5   Phase coherence and self-averaging : universal fluctuations

The measurable physical quantities of a disordered quantum system depend on the specific realization of the disorder, at least so long as the characteristic lengths of the system are smaller than the phase coherence length L_ϕ. In the opposite case, that is, for lengths greater than L_ϕ, the phase coherence is lost, and the system becomes classical, namely the physical quantities are independent of the specific realization of the disorder. The physics of systems of size less than L_ϕ, called *mesoscopic systems* [5], is thus particularly interesting because of coherence effects [9, 10]. The physics of mesoscopic systems makes precise the distinction between the complexity due to disorder described by l_e and the decoherence, which depends on L_ϕ :

- Disorder (l_e) : loss of symmetry and of good quantum numbers (complexity).

- Loss of phase coherence (L_ϕ).

Let us now attempt to understand why a disordered quantum system larger than L_ϕ exhibits self-averaging, *i.e.*, why its measurable physical properties are equal to their ensemble averages. If the characteristic size L of a system is much greater than L_ϕ, the system may be decomposed into a collection of $N = (L/L_\phi)^d \gg 1$ statistically independent subsystems, in each of which the quantum coherence is preserved. A physical quantity defined in each subsystem will then take on N random values. The law of large numbers ensures that every macroscopic quantity is equal, with probability one, to its average value. Consequently, every disordered system of size $L \gg L_\phi$ is effectively equivalent to an ensemble average. On the other hand, deviations from self-averaging are observed in systems of sizes smaller than L_ϕ because of the underlying phase coherence. The study of these deviations is one of the main goals of mesoscopic physics. Consider the particularly important example of fluctuations in the electrical conductance of a weakly disordered metal (Chapter 11). In the classical self-averaging limit, for a cubic sample of size L, the relative conductance fluctuations vary as $1/\sqrt{N}$:

$$\frac{\sqrt{\overline{\delta G^2}}}{\overline{G}} \simeq \frac{1}{\sqrt{N}} \simeq \left(\frac{L_\phi}{L}\right)^{d/2} \tag{1.9}$$

where $\delta G = G - \overline{G}$. The average conductance $\overline{G}$ is the classical conductance G_{cl} given by Ohm's law $G_{cl} = \sigma L^{d-2}$ where σ is the electrical conductivity [6]. From relation (1.9), we deduce that $\overline{\delta G^2} \propto L^{d-4}$. For $d \leq 3$, the fluctuations go to zero in the large scale limit, and the system is said to be self-averaging. In contrast, for $L < L_\phi$, it is found experimentally that

$$\sqrt{\overline{\delta G^2}} \simeq const. \times \frac{e^2}{h} \ . \tag{1.10}$$

---

[5]The Greek root $\mu\epsilon\sigma o\varsigma$ means intermediate.

[6]The expression $G_{cl} = \sigma L^{d-2}$ is a generalization to d dimensions of the standard expression $G_{cl} = \sigma S/L$, for a sample of length L and cross section S.

In the mesoscopic regime, the amplitude of conductance fluctuations is independent of the size L and of the amount of disorder, and one speaks of *universal conductance fluctuations*. The variance of the conductance is the product of a universal quantity e^2/h and a numerical factor which depends solely on the sample geometry. This implies that in the mesoscopic regime, the electrical conductance is no longer a self-averaging quantity. This universality is shown in Figure 1.11 where each plot corresponds to a very different system. One essential characteristic of mesoscopic fluctuations is their *reproducibility*. For a given realization of disorder, the dependence of the fluctuations as a function of an external parameter such as Fermi energy or magnetic field is perfectly reproducible. In this sense, the fluctuations represent, just like speckle patterns in optics, a *"fingerprint"* of the realization of the disorder, and uniquely characterize it.
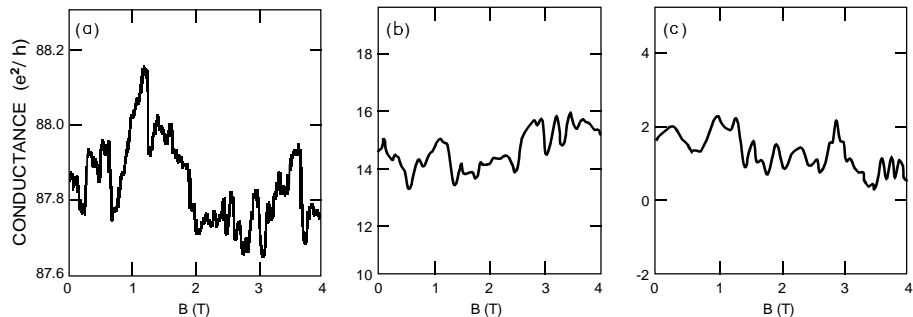

Figure 1.11: *Aperiodic variations in the magnetoconductance of three different systems. a) A gold ring of diameter 0.8 mm, b) a Si-MOSFET sample, and c) the result of numerical simulations of the disordered Anderson model (discussed in Chapter 2). The conductance varies by several orders of magnitude from one system to another, but the fluctuations remain of order e^2/h (P.A. Lee et al., Phys. Rev. B* **35***, 1039 (1987)).*

1.6   Spectral correlations

We have mentioned the signature of coherent effects on transport properties such as electrical conductance or albedo. For an *isolated* system of finite size, we may wonder about the effect of disorder on the spatial behavior of wave functions and on the correlation of eigenenergies. For electromagnetic waves, we are interested in the spectrum of eigenfrequencies. If, for instance, the wave functions are strongly affected by the disorder and are exponentially localized, then the corresponding eigenenergies (or frequencies) may be arbitrarily close one to another since they describe states for which the spatial overlap is exponentially small. These wave functions are uncorrelated as are their energy levels. If, on the other hand, the wavefunctions are spatially delocalized over the system and do not exhibit any spatial structure, which corresponds to a

regime we may consider as *ergodic*, then the important spatial overlap of the eigenfunctions induces spectral correlations manifested by a "repulsion" of the energy levels. These two extreme situations are very general, and are insensitive to the microscopic details characterizing the disorder. It turns out that the spectral correlations present *universal properties* common to very different physical systems. Consider, for example, the probability $P(s)$ that two neighboring energy levels are separated by s. The two preceding situations are described by two robust limiting cases for the function $P(s)$, corresponding, respectively, to a *Poisson* distribution for the exponentially localized states, and to a *Wigner-Dyson* distribution for the ergodic case. These two distributions, represented in Figure 10.1, describe a wide range of physical problems and divide them, to first approximation, into two classes, corresponding either to integrable systems (Poisson) or to non-integrable –also called *chaotic*– systems (Wigner-Dyson). This latter case may be systematically studied by using *random matrix theory* along the general lines discussed in Chapter 10.

Of course, a complex medium exhibits such universal behavior only in limiting cases. From the methods developed in this book, we shall see how to recover certain results of random matrix theory, and to identify corrections to the universal regime. These spectral correlations are extremely sensitive to the loss of phase coherence. They thus depend on L_ϕ and are characteristic of the mesoscopic regime. They are evidenced by the behavior of thermodynamic variables such as magnetization or persistent currents which constitute the orbital response of electrons to an applied magnetic field; this is the object of Chapter 14.

1.7 Classical probability and quantum crossings

Most physical quantities studied in this book are expressed as a function of the product of two complex amplitudes, each being the sum of contributions associated with multiple scattering trajectories :

$$\sum_i a_i^* \sum_j a_j = \sum_{i,j} a_i^* a_j \ . \tag{1.11}$$

This is the case, for example, of light intensity considered in section 1.4. The combination of amplitudes (1.11) is related to the *probability of quantum diffusion*, whose role is essential in characterizing the physical properties of disordered media. This probability, which describes the evolution of a wave packet between any two points $\boldsymbol{r}$ and $\boldsymbol{r}'$, is written as the product of two complex amplitudes [7] known as propagators or Green's functions. Denoting the average probability by $P(\boldsymbol{r}, \boldsymbol{r}')$, we have

$$P(\boldsymbol{r}, \boldsymbol{r}') \propto \overline{\sum_{i,j} a_i^*(\boldsymbol{r}, \boldsymbol{r}') a_j(\boldsymbol{r}, \boldsymbol{r}')} \ . \tag{1.12}$$

---

[7] In this introduction, we do not seek to establish exact expressions for the various physical quantities, but simply to discuss their behavior as a function of multiple scattering amplitudes. We therefore omit time or frequency dependence when it is not essential. More precise definitions are left for Chapters 3 and 4.

Each amplitude $a_j(\boldsymbol{r},\boldsymbol{r}')$ describes a propagating trajectory j from $\boldsymbol{r}$ to $\boldsymbol{r}'$, and thus $P(\boldsymbol{r},\boldsymbol{r}')$ appears as the sum of contributions of pairs of trajectories, each characterized by an amplitude and a phase. This sum may be decomposed into two contributions, one for which the trajectories i and j are identical, the other for which they are different :

$$P(\boldsymbol{r},\boldsymbol{r}') \propto \overline{\sum_j |a_j(\boldsymbol{r},\boldsymbol{r}')|^2} + \overline{\sum_{i \neq j} a_i^*(\boldsymbol{r},\boldsymbol{r}')a_j(\boldsymbol{r},\boldsymbol{r}')} \ . \tag{1.13}$$

In the former contribution the phases vanish. In the latter, the dephasing of
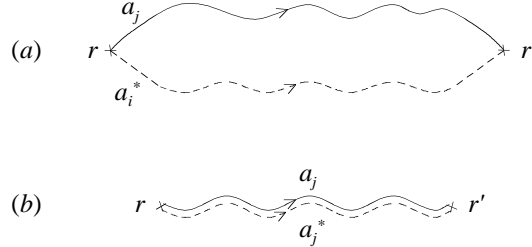

Figure 1.12: *By averaging over disorder, the contribution from pairs of different trajectories (a) vanishes, leaving only terms corresponding to identical trajectories to contribute to the average probability (b).*

paired trajectories is large and random, and consequently their contribution vanishes on average [8]. The probability is thus given by a sum of intensities and does not contain any interference term (Figure 1.12) :

$$P_{cl}(\boldsymbol{r},\boldsymbol{r}') \propto \overline{\sum_j |a_j(\boldsymbol{r},\boldsymbol{r}')|^2} \ . \tag{1.14}$$

We shall call this classical term a *Diffuson*. In the weak disorder limit, that is, as long as the wavelength λ is small compared to the elastic mean free path l_e, and for length scales larger than l_e, the Diffuson is well-described by the solution of the diffusion equation

$$\left[\frac{\partial}{\partial t} - D\Delta\right] P_{cl}(\boldsymbol{r},\boldsymbol{r}',t) = \delta(\boldsymbol{r} - \boldsymbol{r}')\delta(t) \ , \tag{1.15}$$

where $D = vl_e/d$ is the diffusion constant, v the group velocity of the wave packet, and d the dimension of space.

One quantity of particular importance is the probability of return to the initial point $P_{cl}(\boldsymbol{r},\boldsymbol{r},t)$, as well as its integral over space $Z(t)$. This last quantity is expressed as a function of the eigenfrequencies denoted E_n associated with the diffusion equation (1.15)

$$Z(t) = \int d\boldsymbol{r}\, P_{cl}(\boldsymbol{r},\boldsymbol{r},t) = \sum_n e^{-E_n t} \tag{1.16}$$

---

[8]We show in the following section that the interference terms of expression (1.13) do not vanish completely, and are at the origin of most of the quantum effects described in this book.

for $t > 0$. For example, for a system [9] of volume Ω, we have

$$Z(t) = \frac{\Omega}{(4\pi Dt)^{d/2}} \quad .\tag{1.17}$$

The dependence as a function of the space dimensionality d plays an essential role, and the physical properties are accordingly more sensitive to the effects of multiple scattering when the dimensionality is small, since the return probability increases with decreasing d.

For a finite system of volume $\Omega = L^d$, boundary conditions may play an important role, since they reflect the nature of the coupling to the environment on which $Z(t)$ depends. This introduces a new characteristic time

$$\tau_D = L^2/D\tag{1.18}$$

called the diffusion time or *Thouless time*. It represents the time to diffuse from one boundary of the sample to the other. If $t \ll \tau_D$, the effect of boundaries is not felt, the diffusion is free and expressed by relation (1.17). If, on the other hand, $t \gg \tau_D$, the entire volume is explored by the random walk, we are in the *ergodic* regime, and $Z(t) \simeq 1$. A characteristic energy is associated with τ_D and it is called the *Thouless energy* $E_c = \hbar/\tau_D$.

1.7.1 Quantum crossings

Taking the second contribution of (1.13) to be zero amounts to neglecting all interference effects. In fact, even after averaging over disorder, this contribution is not rigorously zero. There still remain terms describing pairs of distinct trajectories, $i \neq j$, which are sufficiently close that their dephasing is small. As an example, consider the case of Figure 1.13.*a*, where the two trajectories in a Diffuson follow the same sequence of scatterings but cross, forming a loop with counter propagating trajectories [10]. This notion of crossing is essential because it is at the origin of coherent effects like weak localization, long range light intensity correlations, or universal conductance fluctuations. As such, it is useful to develop intuition about them. Figures 1.13.*a,b* show that one such crossing mixes four complex amplitudes and pairs them in different ways. The crossing, also called *Hikami box*, is an object whose role is to permute amplitudes [14]. For the induced dephasing to be smaller than 2π, the trajectories must be as close to each other as possible, and the crossing must be localized in space, that is, on a scale of the order of the elastic mean free path l_e. We shall see that the volume associated with a crossing in d dimensions is of order $\lambda^{d-1} l_e$. This may be interpreted by attributing a length vt to a Diffuson – the object built with paired trajectories - propagating during a time t, where v is the group velocity, and a cross section λ^{d-1}, giving a volume $\lambda^{d-1} vt$.

To evaluate the importance of quantum effects, let us estimate the probability that two Diffusons will cross, as in Figure 1.13.*b*. This probability, for

---

[9]We ignore boundary effects, and thus are dealing with free diffusion.

[10]These quantum crossings, which exchange two amplitudes, should not be confused with the self-crossings of a classical random walk.
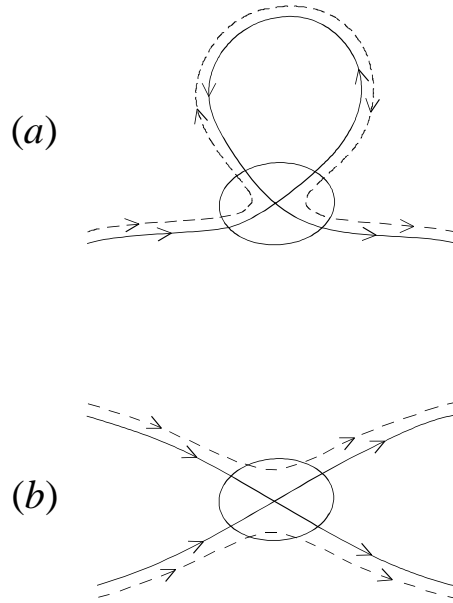
Figure 1.13: *a) The crossing of trajectories contributing to a Diffuson leads to a new pairing of amplitudes. b) The pairing of four amplitudes resulting from the crossing of two Diffusons.*

a time interval dt, is proportional to the ratio of the Diffuson volume to the system volume $\Omega = L^d$, that is,

$$dp_\times(t) = \frac{\lambda^{d-1}vdt}{\Omega} \simeq \frac{1}{g}\frac{dt}{\tau_D} \quad . \tag{1.19}$$

In this expression, we have explicitly indicated the diffusion time $\tau_D = L^2/D$. We have also introduced a dimensionless number g, proportional to the inverse ratio of the two volumes $\lambda^{d-1}v\tau_D/\Omega$. We will show that this number is none other than the classical electrical conductance $g = G_{cl}/(e^2/h)$, in units of the quantum of conductance e^2/h (relation 7.22).

When the disordered medium is coupled to leads, the diffusing waves escape from the system in a time of the order of τ_D which sets therefore the characteristic time for diffusive trajectories. Therefore, the probability for a crossing during the time τ_D is inversely proportional to the dimensionless conductance, namely

$$p_\times(\tau_D) = \int_0^{\tau_D} dp_\times(t) \simeq \frac{1}{g} \quad . \tag{1.20}$$

This parameter allows us to evaluate the importance of quantum corrections to the classical behavior. In the limit of weak disorder $\lambda \ll l_e$, the conductance g is large, so the crossing probability, and hence the effects of coherence, are small.

The quantum crossings, and the dephasing which they induce, introduce a correction to the classical probability (1.14). It is the combination of these

crossings, the interference that they describe, and the spatially long range nature of the Diffuson, which allows to propagate coherent effects over the entire system. Those are the effects which lie at the basis of mesoscopic physics. The simple argument developed here straightforwardly implies that the quantum corrections to classical electron transport are of the order $G_{cl} \times 1/g$, that is to say, e^2/h.

In the limit of weak disorder, the crossings are independent of each other. This allows us to write successive corrections to the classical probability as a function of the number of crossings, that is, as a power series in $1/g$.

1.8 Objectives

This book deals with coherent multiple scattering of electronic or electromagnetic waves in disordered media, in the limit where the wavelength [11] $\lambda = 2\pi/k$ is small compared to the elastic mean free path l_e. This is the limit of weak disorder. It is possible to develop a general framework for the description of a large number of physical phenomena, which were effectively predicted, observed, and explained, by employing a small number of rather general ideas. In this section, we briefly outline these ideas, and indicate the relevant chapter in which these phenomena are discussed.

● **Weak localization corrections to the conductivity (Chap. 7) and the coherent backscattering peak (Chap. 8)**

One particularly important example where the notion of quantum crossing appears is that of electron transport in a weakly disordered conductor. Consider, for example, transport across a sample of size L. The conductance corresponding to the classical probability is the classical or Drude conductance G_{cl}. The quantum correction to the probability leads to a correction to the conductance.

This correction associated with a single crossing is of order $1/g$, but it depends as well on the distribution of loops, that is, on the closed diffusive trajectories (Figure 1.14), whose number is given by the spatial integral (1.16), namely by the integrated probability of returning to the origin $Z(t)$. The probability $p_o(\tau_D)$ of crossing the sample with a single quantum crossing (one loop) is of the form

$$p_o(\tau_D) \sim \frac{1}{g} \int_0^{\tau_D} Z(t) \, \frac{dt}{\tau_D} \quad , \tag{1.21}$$

where $\tau_D = L^2/D$. We obtain the relative correction to the average conductance $\Delta G = G - G_{cl}$ as,

$$\boxed{\frac{\Delta G}{G_{cl}} \sim -p_o(\tau_D)} \tag{1.22}$$

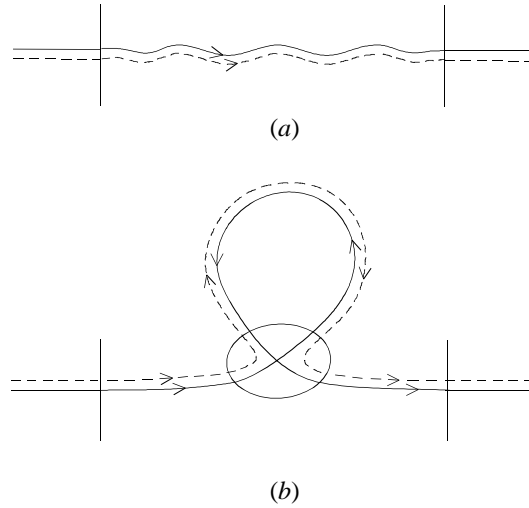[11]For electrons, λ is the Fermi wavelength.

Figure 1.14: *The crossing of a Diffuson with itself (b) leads to a quantum correction to the classical Drude conductivity (a).*

The minus sign in this correction indicates that taking a quantum crossing and therefore a closed loop into account has the effect of reducing the average conductance. This is called the *weak localization* correction.

We note that the two multiple scattering trajectories that form a loop evolve in *opposite* directions. If the system is time reversal invariant, the two amplitudes associated to these trajectories j and j^T are identical $a_{j^T}(\boldsymbol{r}, \boldsymbol{r}) = a_j(\boldsymbol{r}, \boldsymbol{r})$ so that their product is equal to the product of two amplitudes propagating in the same direction. If there are processes which break this invariance, then the weak localization correction vanishes. This pairing of time-reversed conjugate trajectories is called a *Cooperon*.

This pairing closely resembles that described in the optical counterpart of section 1.4 and Figure 1.10.*b*, which corresponds to time reversed multiple scattering amplitudes $a_j(\boldsymbol{r}_1, \boldsymbol{r}_2)$ and $a_{j^T}^*(\boldsymbol{r}_1, \boldsymbol{r}_2)$. For the geometry of a semi-infinite disordered medium, and a plane wave incident along the direction $\boldsymbol{k}$ which emerges along $\boldsymbol{k}'$, the average reflected intensity $I(\boldsymbol{k}, \boldsymbol{k}')$ (also called the average *albedo*) depends on the angle between the directions $\boldsymbol{k}$ and $\boldsymbol{k}'$. From (1.8), we have

$$I(\boldsymbol{k}, \boldsymbol{k}') \propto \int d\boldsymbol{r} d\boldsymbol{r}' P_{cl}(\boldsymbol{r}, \boldsymbol{r}') \left[1 + e^{i(\boldsymbol{k}+\boldsymbol{k}') \cdot (\boldsymbol{r}-\boldsymbol{r}')} \right] \qquad (1.23)$$

We identify $\overline{|f(\boldsymbol{r}, \boldsymbol{r}')|^2}$ with the Diffuson $P_{cl}(\boldsymbol{r}, \boldsymbol{r}')$ whose endpoints $\boldsymbol{r}$ and $\boldsymbol{r}'$ are taken to be close to the interface between the diffusive medium and the vacuum. The first term in the brackets is the phase-independent classical contribution, while the interference term has an angular dependence around the

backscattering direction $\boldsymbol{k}' \simeq -\boldsymbol{k}$. The albedo therefore exhibits a peak in this direction, called the *coherent backscattering peak*, whose intensity is twice the classical value.

• **Correlations in speckle patterns (Chap. 12)**

For a given realization of disorder, the intensity distribution of a light wave undergoing multiple scattering is a random distribution of dark and bright spots (Figure 1.2) called a speckle pattern. This interference pattern, arising from the superposition of complex amplitudes, constitutes a "fingerprint" of the specific disorder configuration. In order to characterize a speckle pattern, we may measure the angular distribution of the transmitted (or reflected) intensity using the geometry of a slab of thickness L. In this case, one measures the normalized intensity $\mathcal{T}_{ab}$ transmitted in the direction $\hat{\boldsymbol{s}}_b$ and corresponding to a wave incident in the direction $\hat{\boldsymbol{s}}_a$ (see Figure 12.2). On average, the transmission coefficient $\overline{\mathcal{T}_{ab}}$ depends only slightly on the directions $\hat{\boldsymbol{s}}_a$ and $\hat{\boldsymbol{s}}_b$, and we denote it $\overline{\mathcal{T}}$. The angular correlation of the speckle is defined by

$$C_{aba'b'} = \frac{\overline{\delta\mathcal{T}_{ab}\delta\mathcal{T}_{a'b'}}}{\overline{\mathcal{T}}^2} \quad , \tag{1.24}$$

where $\delta\mathcal{T}_{ab} = \mathcal{T}_{ab} - \overline{\mathcal{T}}$. The fluctuations of the speckle, for a given incidence direction $\hat{\boldsymbol{s}}_a$, are described by the quantity $C_{abab} = \overline{\delta^2\mathcal{T}_{ab}}/\overline{\mathcal{T}}^2$ which happens, as we shall see, to be equal to 1, yielding

$$\overline{\mathcal{T}_{ab}^2} = 2\,\overline{\mathcal{T}}^2 \ . \tag{1.25}$$

This result, which constitutes the *Rayleigh law*, describes the most "visible" aspect of a speckle pattern, namely, its "granularity," with relative fluctuations of the order of unity.

In contrast to the probability (average conductance or light intensity), a correlation function such as (1.24) is the product of *four complex amplitudes* (Figure 1.15.*a*). When averaging over disorder, the only important contributions are obtained by pairing these amplitudes so as to form Diffusons or Cooperons. Neglecting, in a first step, the possibility of a quantum crossing of two Diffusons, there are two possibilities, shown in Figures 1.15.*b,c*. The first is the product of two average intensities $\overline{\mathcal{T}_{ab}}$ and $\overline{\mathcal{T}_{a'b'}}$. The second gives the principal contribution to the correlation function (1.24), denoted $C_{aba'b'}^{(1)}$. It is nonzero only if $\hat{\boldsymbol{s}}_a - \hat{\boldsymbol{s}}_{a'} = \hat{\boldsymbol{s}}_b - \hat{\boldsymbol{s}}_{b'}$ and it decays exponentially as a function of $k|\hat{\boldsymbol{s}}_a - \hat{\boldsymbol{s}}_{a'}|/L$, that is, over a very small angular range.

It is also possible to pair the amplitudes by interposing one or more quantum crossings. This results in corrections to the angular correlation function in powers of $1/g$. The first one, denoted $C_{aba'b'}^{(2)}$, has a *single crossing*, and is shown in Figure 1.15.*d*. The presence of a crossing imposes constraints on the pairing of the amplitudes, and thus gives rise to a different angular dependence. We will show in section 12.4.2 that $C_{aba'b'}^{(2)}$ decays as a power of $k|\hat{\boldsymbol{s}}_a - \hat{\boldsymbol{s}}_{a'}|/L$, instead of an exponential decay. It has a weight $1/g \ll 1$ as compared to the term with no crossing.
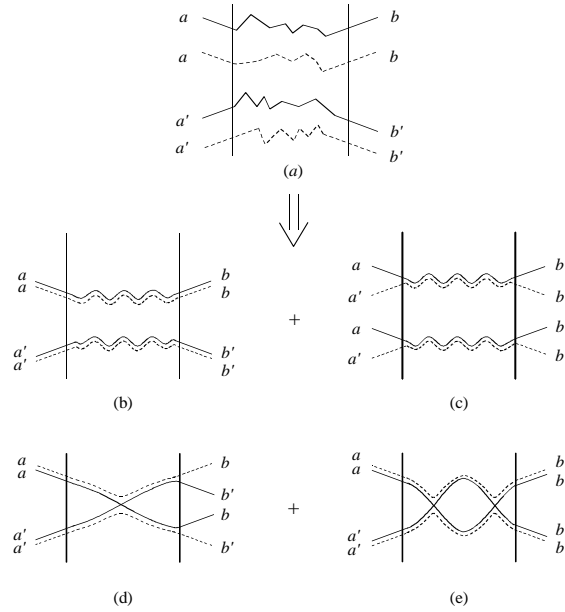
Figure 1.15: *(a) The angular correlation function of a speckle pattern is built from the product of four complex amplitudes corresponding to four plane waves incoming along directions $\hat{\mathbf{s}}_a$ and $\hat{\mathbf{s}}_{a'}$ and emerging along $\hat{\mathbf{s}}_b$ and $\hat{\mathbf{s}}_{b'}$. The main contributions are obtained by pairing the amplitudes two by two to form Diffusons. This gives rise to contributions (b) and (c). Contribution (c), which corresponds to the correlation function $C^{(1)}_{aba'b'}$ decays exponentially in angle. Contribution (d) contains one quantum crossing, while (e) has two quantum crossings. In this last case, we note that the corresponding correlation function has no angular dependence.*

The contribution $C^{(3)}_{aba'b'}$, with *two crossings* is sketched in Figure 1.15.*e*. Because of the two-crossing structure, this contribution has no angular dependence; *i.e.*, it yields a uniform background to the correlation function. This result is characteristic of coherent multiple scattering, that is to say, of the combined effect of quantum crossings and of their long range propagation through the Diffusons. Upon averaging the total angular correlation function over all directions of incident and emergent waves, only this last contribution survives, which constitutes the analog for waves of universal conductance fluctuations [11, 12].

• Universal conductance fluctuations (Chap. 11)

These considerations obtained for electromagnetic waves are easily transposed to the case of electrons in a weakly disordered metal, and in this context lead to conductance fluctuations. In the mesoscopic regime, these fluctuations differ considerably from the classical result : they are universal and of order e^2/h (see section 1.5). This results from the existence of quantum crossings.

More precisely, the calculation of the fluctuations $\overline{\delta G^2} = \overline{G^2} - \overline{G}^2$ involves the pairing of four complex amplitudes paired into two Diffusons. Moreover, in the framework of the Landauer formalism (Appendix C7.2), the conductance, in units of e^2/h, is related to the transmission coefficient $\mathcal{T}_{ab}$ summed over all incident and emergent directions a and b. Thus, as for the speckle angular correlations, it may be shown that the term with no quantum crossing corresponds to $\overline{G}^2$. The contribution from a single crossing vanishes upon summation over the emergent directions. In contrast, the term with two quantum crossings has no angular dependence (Figure 1.15.e) and it gives a universal variance $\overline{\delta G^2}$ proportional to $G_{cl}^2/g^2 = (e^2/h)^2$.

We note that, as for the weak localization correction, the variance $\overline{\delta G^2}$ depends on the distribution of *loops*. Here the loops result from *two crossings* (Figure 1.15e). For a loop of length vt, the choice of the relative position of the two crossings introduces an additional factor $\lambda^{d-1}vt/\Omega \simeq t/(g\tau_D)$ in the integral (1.21). We thus deduce that

$$
\boxed{\frac{\overline{\delta G^2}}{G_{cl}^2} \sim \frac{1}{g^2} \int_0^{\tau_D} Z(t)\frac{tdt}{\tau_D^2}}
\tag{1.26}
$$

This expression is similar to the relative correction of weak localization (1.21, 1.22), but the additional factor t has important consequences. The dependence $Z(t) \propto t^{-d/2}$ of the integrated return probability to the origin implies that weak localization correction is universal for $d < 2$, while conductance fluctuations are universal for $d < 4$.

• Dephasing (Chap. 6)

The interference effects discussed earlier result from the existence of quantum crossings. They depend on the coherence of the wave-scatterer system, and may be modified in the presence of dephasing processes. Such processes are related to additional degrees of freedom which we may divide into three classes, examples of which are :

• External field : uniform magnetic field, Aharonov-Bohm flux.

• Degrees of freedom of the scattered wave : electron spin and photon polarization.

• Degrees of freedom of the scatterers : magnetic impurities, environment induced by other electrons, motion of scatterers, internal quantum degrees of freedom (atomic Zeeman sublevels).

Let us first consider the case of multiple scattering of electrons, now in the presence of a magnetic field. Full coherence implies that time-reversed trajectories have the same amplitude. This is no longer the case in the presence of a magnetic field, which induces a dephasing between conjugate trajectories :

$$
a_{j^T}(\boldsymbol{r},\boldsymbol{r}') = a_j(\boldsymbol{r},\boldsymbol{r}')e^{i\Phi_j(\boldsymbol{r},\boldsymbol{r}')} \ .
\tag{1.27}
$$

Using (1.13) and the discussion on page 33, the correction to the return probability associated to the Cooperon, which we denote P_c, is of the form

$$P_c(\boldsymbol{r},\boldsymbol{r}) \propto \overline{\sum_j |a_j(\boldsymbol{r},\boldsymbol{r})|^2 e^{i\Phi_j(\boldsymbol{r},\boldsymbol{r})}} \quad , \tag{1.28}$$

where $\Phi_j(\boldsymbol{r},\boldsymbol{r})$ is the phase difference accumulated along the closed trajectories. The dephasing due to a magnetic field is

$$\Phi_j(\boldsymbol{r},\boldsymbol{r}') = \frac{2e}{\hbar} \int_{\boldsymbol{r}}^{\boldsymbol{r}'} \boldsymbol{A}.d\boldsymbol{l} \quad , \tag{1.29}$$

where the factor 2 comes from the fact that the two paired trajectories each accumulate the same phase, but with opposite signs, so that their difference adds. The coherent contribution to the return probability is thus affected by this phase factor, and the weak localization correction to the electrical conductance takes the form

$$\boxed{\frac{\Delta G}{G_{cl}} \propto - \int dt Z(t) \left\langle e^{i\Phi(t)} \right\rangle} \tag{1.30}$$

where $\left\langle e^{i\Phi(t)} \right\rangle$ is the average phase factor of the ensemble of trajectories of length vt.

The magnetic field thus appears as a way to probe phase coherence. In particular, the Aharonov-Bohm effect gives rise to the spectacular Sharvin-Sharvin effect, in which the average conductance still has a contribution which oscillates with period $h/2e$ (section 7.6.2). To evaluate the coherent contribution in the presence of a magnetic field, we must look for solutions of the *covariant diffusion equation* which replaces (1.15)

$$\left[\frac{\partial}{\partial t} - D\left(\nabla_{\boldsymbol{r}} + i\frac{2e}{\hbar}\boldsymbol{A}(\boldsymbol{r})\right)^2\right] P(\boldsymbol{r},\boldsymbol{r}',t) = \delta(\boldsymbol{r}-\boldsymbol{r}')\delta(t) \ . \tag{1.31}$$

The dephasing (1.29) resulting from the application of a magnetic field changes the phase accumulated along a multiple scattering trajectory. In contrast, to describe the coupling to other degrees of freedom, we are led to locally average the relative dephasing between the two complex amplitudes which interfere. This results from our incomplete knowledge of the internal quantum state of the scatterers. The average over the scatterers degrees of freedom gives rise to an irreversible dephasing, which we describe using a finite phase coherence time τ_ϕ. We show in Chapter 6 that the contributions of the Diffuson and the Cooperon are modified by a phase factor which in general decreases exponentially with time.

$$\left\langle e^{i\Phi(t)} \right\rangle \propto e^{-t/\tau_\phi}. \tag{1.32}$$

Here $\langle \cdots \rangle$ indicates an average over both disorder and these other degrees of freedom. The determination of the phase coherence time requires the evaluation

of the average in (1.32). This notion of dephasing extends to any perturbation whose effect is to modify the phase relation between paired multiple scattering trajectories. We present such an example just below.

● **Dynamics of scatterers - diffusing wave spectroscopy (Chaps. 6 and 9)**

When properly understood, a source of dephasing is not necessarily a nuisance, but may be used to study the properties of the diffusive medium. Thus, in the case of scattering of electromagnetic waves, it is possible, by measuring the time autocorrelation function of the electromagnetic field, to take advantage of the coherent multiple scattering to deduce information about the dynamics of the scatterers which is characterized by a time scale τ_b. In fact, since the scatterer velocity is usually much smaller than that of the wave, if we send light pulses at different times, 0 and T, we can probe different realizations of the random potential. The paired trajectories thus explore different configurations separated by a time T. This results in a dephasing which depends on the motion of the scatterers during the time interval T. The time correlation function of the electric field E at a point $\boldsymbol{r}$ (with a source at $\boldsymbol{r}_0$) is of the form

$$\langle E(\boldsymbol{r},T)E^*(\boldsymbol{r},0)\rangle \propto \left\langle \sum_j a_j(\boldsymbol{r}_0,\boldsymbol{r},T)a_j^*(\boldsymbol{r}_0,\boldsymbol{r},0)\right\rangle \ , \qquad (1.33)$$

where the average is over both the configurations and the motion of the scatterers. It is given as a function of the classical probability (the Diffuson) :

$$\boxed{\langle E(\boldsymbol{r},T)E^*(\boldsymbol{r},0)\rangle \propto \int_0^\infty dt P_{cl}(\boldsymbol{r}_0,\boldsymbol{r},t)e^{-t/\tau_s}} \qquad (1.34)$$

The characteristic time τ_s, which depends on the dynamics of the scatterers, is related to τ_b and to T. This technique which consists in measuring the time correlations of the field or the intensity is known as *diffusing wave spectroscopy*. It gives information about the dynamics of the scatterers. Since the long multiple scattering paths decorrelate very quickly, we may obtain information about the dynamics at very short times. This idea is largely used in the study of turbid media.

● **Density of states (Chap. 10)**

The preceding examples dealt with the transport of waves or electrons. The case of thermodynamic quantities is more delicate, since they are expressed as a function of the density of states, which has the form

$$\rho(\epsilon) \propto \int d\boldsymbol{r} \sum_j a_j(\boldsymbol{r},\boldsymbol{r}) \ . \qquad (1.35)$$

When averaging over disorder, the phases vanish, and there is no remnant of phase coherence. On the other hand, quantities which are products of densities of states or thermodynamic potentials involve *pairs of trajectories* and are

therefore sensitive to the effects of phase coherence. For example, the *fluctuations of the density of states* are of the form

$$\overline{\rho(\epsilon)\rho(\epsilon')} \propto \int dr dr' \overline{\sum_{i,j} a_i(\boldsymbol{r},\boldsymbol{r}) a_j^*(\boldsymbol{r}',\boldsymbol{r}')} \quad , \tag{1.36}$$

i.e., they involve paired closed trajectories but with different initial points. In order to keep them paired, we notice that in the integration over initial points there appears the length $\mathcal{L}_i$ of each multiple scattering closed loops. We thus obtain a structure quite close to the classical probability (1.14) :

$$\overline{\rho(\epsilon)\rho(\epsilon')} \propto \int d\boldsymbol{r} \overline{\sum_i \mathcal{L}_i |a_i(\boldsymbol{r},\boldsymbol{r})|^2} \tag{1.37}$$

but which contains, besides $P_{cl}(\boldsymbol{r},\boldsymbol{r},t)$, the length $\mathcal{L}_i$ of the trajectories, which is proportional to vt. More precisely, the Fourier transform (with respect to $\epsilon - \epsilon'$) of the correlation function $\overline{\rho(\epsilon)\rho(\epsilon')}$ is proportional not to $Z(t)$ but to $t\,Z(t)$:

$$\boxed{\overline{\rho(\epsilon)\rho(\epsilon')} \xrightarrow{F.T.} t\,Z(t)} \tag{1.38}$$

The number of levels $N(E)$ in an energy interval E is the integral of the density of states. A particularly useful quantity for the characterization of the spectral correlations is the variance $\Sigma^2(E) = \overline{N^2} - \overline{N}^2$ of this number of levels given by

$$\Sigma^2(E) = \frac{2}{\pi^2} \int_0^\infty dt \frac{Z(t)}{t} \sin^2(\frac{Et}{2}) \quad . \tag{1.39}$$

For energies less than the Thouless energy E_c, that is, for times greater than τ_D, we are in the ergodic regime and $Z(t) = 1$. Starting from (1.39), we get

$$\Sigma^2(E) \propto \ln E \quad . \tag{1.40}$$

We recover the behavior of the spectral rigidity described by *random matrix theory*. In the opposite limit, when $E \gg E_c$, that is $t \ll \tau_D$, $Z(t)$ depends on the spatial dimension d via expression (1.17), which leads to the non-universal behavior of the variance $\Sigma^2(E) \propto (E/E_c)^{d/2}$. We thus see the role diffusion plays in spectral properties. It is, in principle, possible to determine the Thouless energy and the diffusion coefficient starting from the spectral correlations. Moreover, these spectral properties enable us in principle to distinguish between a good and a poor conductor.

• Fluctuations in thermodynamic properties - orbital magnetism (Chap. 14)

The orbital magnetization of an electron gas is given by the derivative of the total energy with respect to the magnetic field :

$$\mathcal{M} \propto -\frac{\partial}{\partial B} \int_{-\epsilon_F}^0 \epsilon \rho(\epsilon, B) d\epsilon \quad . \tag{1.41}$$

In the geometry of a ring threaded by a magnetic field, this magnetic response corresponds to the existence of a *persistent current* circulating along the ring. The fluctuations of the magnetization may be calculated simply from the fluctuations of the density of states. Given the definition (1.41), the variance $\overline{\delta\mathcal{M}^2} = \overline{\mathcal{M}^2} - \overline{\mathcal{M}}^2$ takes the form

$$\overline{\delta\mathcal{M}^2} \propto \frac{\partial}{\partial B}\frac{\partial}{\partial B'} \int_{-\epsilon_F}^{0}\int_{-\epsilon_F}^{0} \epsilon\,\epsilon'\overline{\rho(\epsilon,B)\rho(\epsilon',B')}d\epsilon d\epsilon'|_{B'=B} \qquad (1.42)$$

which upon Fourier transformation leads to

$$\boxed{\overline{\delta\mathcal{M}^2} \propto \int_0^\infty \frac{\partial^2 Z(t,B)}{\partial B^2}\frac{e^{-t/\tau_\phi}}{t^3}dt} \qquad (1.43)$$

where the dependence of $Z(t,B)$ on the magnetic field is obtained by solving equation (1.31). Thus, though the average value of the magnetization is not affected by the phase coherence, its distribution is.

- **Coulomb interaction (Chap. 13)**

Until now, we have ignored the Coulomb interaction between electrons. Taking this into account changes numerous physical properties, particularly in the presence of disorder, since the probability that two electrons interact is increased by the diffusive motion of the electrons. For sufficiently high electron densities, the potential is strongly screened and we may describe the effect of the interactions in the Hartree-Fock approximation. It is enough to add an interaction term of the form

$$\frac{1}{2}\int U(\boldsymbol{r}-\boldsymbol{r}')n(\boldsymbol{r})n(\boldsymbol{r}')d\boldsymbol{r}d\boldsymbol{r}' \simeq \frac{U}{2}\int n^2(\boldsymbol{r})d\boldsymbol{r} \qquad (1.44)$$

to the total energy, where $U(\boldsymbol{r}-\boldsymbol{r}') \simeq U\delta(\boldsymbol{r}-\boldsymbol{r}')$ is the screened interaction, and $n(\boldsymbol{r})$ is the local electron density, related to the density of states, so that

$$n(\boldsymbol{r})n(\boldsymbol{r}) \propto \int d\epsilon d\epsilon' \sum_{ij} a_i^*(\boldsymbol{r},\boldsymbol{r},\epsilon)a_j(\boldsymbol{r},\boldsymbol{r},\epsilon') \ . \qquad (1.45)$$

The correction to the total energy has the form

$$\delta E_{ee} \propto U\int d\boldsymbol{r}d\epsilon_1 d\epsilon_2 P_{cl}(\boldsymbol{r},\boldsymbol{r},\epsilon_1-\epsilon_2) \ . \qquad (1.46)$$

This correction gives an additional contribution to the average magnetization which reads

$$\boxed{\mathcal{M}_{ee} \propto -U\int_0^\infty \frac{\partial Z(t,B)}{\partial B}\frac{e^{-t/\tau_\phi}}{t^2}dt} \qquad (1.47)$$

• **Density of states anomaly**

The aforementioned shift in energy (1.46) due to the Coulomb interaction also implies a reduction of the density of states at the Fermi level. Formally, the density of states is expressed as the second derivative of δE_{ee} with respect to the shift ϵ measured relative to the Fermi level which, using (1.46), yields

$$\delta\rho(\epsilon) \propto U \int d\boldsymbol{r}\, P_{cl}(\boldsymbol{r},\boldsymbol{r},\epsilon) \tag{1.48}$$

or

$$\boxed{\delta\rho(\epsilon) \propto U \int_0^\infty Z(t)\cos\epsilon t\ dt} \tag{1.49}$$

This correction, called *density of states anomaly*, is an important signature of the electron-electron interaction, and it depends on the space dimensionality and the sample geometry via the probability $Z(t)$.

• **Quasiparticle lifetime (Chap. 13)**

The lifetime of a single particle electronic state is limited by electron-electron interaction. Using the Fermi golden rule, it is shown that it is related to the square of a matrix element of the screened Coulomb interaction, that is, a product of four wavefunctions. The average over disorder introduces the probability of return to the origin. We will show that

$$\boxed{\frac{1}{\tau_{ee}(\epsilon)} \propto \int_0^\infty \frac{Z(t)}{t} \sin^2\frac{\epsilon t}{2} dt} \tag{1.50}$$

where ϵ is the energy shift measured from the Fermi level. This time can be measured by studying how an electronic current injected at the energy ϵ relaxes to equilibrium. The time $\tau_{ee}(\epsilon)$ diverges as the energy ϵ goes to zero, that is, for a particle at the Fermi level. If it diverges faster than ϵ, then a state at the Fermi level remains well-defined, and we may still use the framework of the Landau theory of Fermi liquids in which, to a good approximation, the electronic states may be regarded as weakly interacting quasiparticle states. At finite temperature, even for $\epsilon = 0$, the time τ_{ee} remains finite, and it therefore contributes to the reduction of phase coherence. Its temperature dependence, denoted $\tau_\phi(T)$, involves the spatial dimension through the diffusive motion.

The Coulomb interaction may also be viewed as that of a single electron coupled to a fluctuating longitudinal electromagnetic field which originates from the other electrons. The phase coherence time $\tau_\phi(T)$ which affects the Cooperon results from the dephasing due to this fluctuating electromagnetic field.

• **Calculational methodology : long and short range correlations - characteristic energies**

To complete and summarize this introduction, we give a survey of the characteristic energy scales of the different regimes we have discussed. In the upper part of Figure 1.16, the ergodic regime corresponds to long times over which the diffusing wave uniformly explores all the volume at its disposal. For shorter times, *i.e.*, for higher energies, diffusion is free, with the boundaries having no effect. We will not consider the regime of times shorter than the average collision time $\tau_e = l_e/v$ for which the motion becomes ballistic. On the lower scale, we indicate the limit of validity of the *Diffuson approximation*, for which quantum corrections are small. These corrections arise predominantly for energies E smaller than the average level spacing Δ.
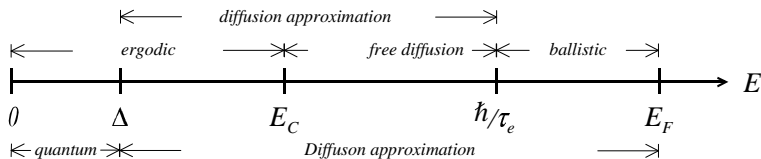

Figure 1.16: *Characteristic energy scales defining the different regimes studied in coherent multiple scattering.*

The calculation of the physical quantities discussed in the aforementioned examples amounts to evaluating the average of a product of amplitudes associated with multiple scattering trajectories. We have seen how these products may be expressed by means of a pairing of either identical amplitudes or time-reversed amplitudes, the other terms averaging to zero. These pairings can be expressed in terms of the diffusion probability, the solution of a diffusion equation (1.15). This is a long range function whose diagrammatic representation is shown in Figure 1.17. All the quantities of interest involve one or more Diffusons. We have also shown that Diffusons may cross, and we have stressed that these quantum crossings are at the origin of the coherent effects observed in multiple scattering. The crossing is described by a short range function which decays exponentially on a scale of order l_e, and preserves the phase coherence between paired trajectories.

We may thus consider the problem of evaluating different physical quantities as a "construction game" which consists in building a diagrammatic representation which facilitates the calculation. The building blocks in this "game" are the Diffusons, Cooperons, and quantum crossings (Hikami boxes). A few examples are presented in Figure 1.17. We will see that the rules of construction are very precise. This notwithstanding, our hope is that the reader, having read this Introduction will acquire an understanding of the principles which guide the construction of various physical quantities.
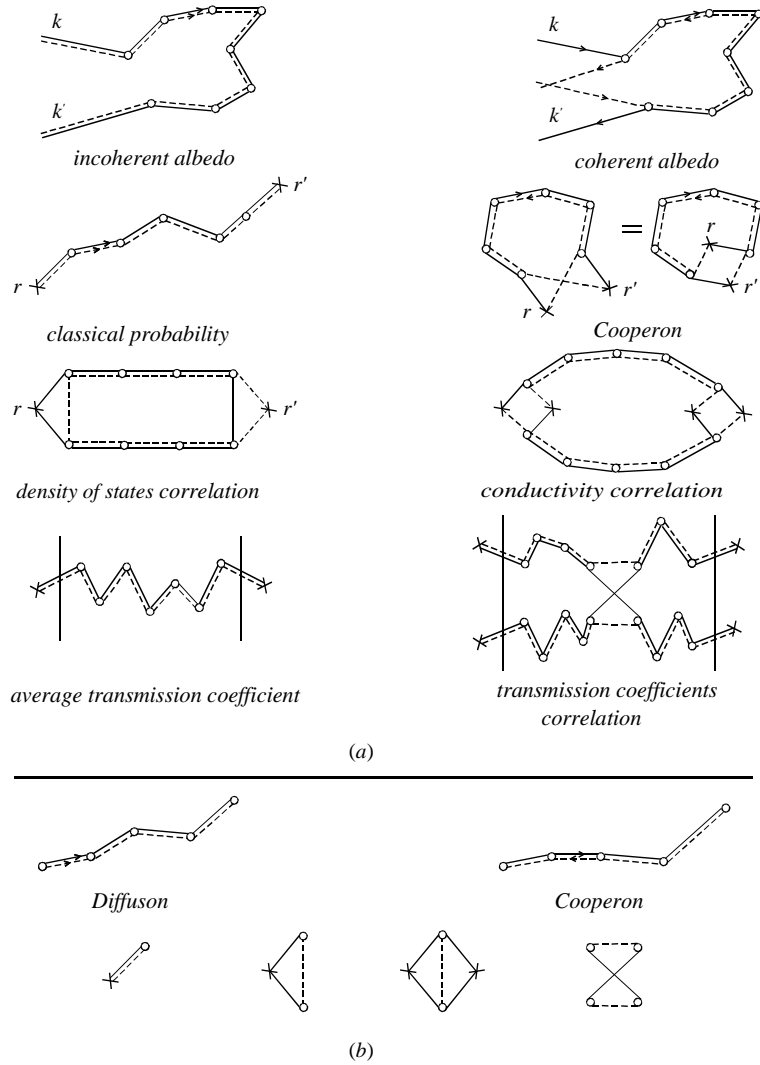
incoherent albedo

coherent albedo

classical probability

Cooperon

density of states correlation

conductivity correlation

average transmission coefficient

transmission coefficients correlation

(*a*)

Diffuson

Cooperon

(*b*)

Figure 1.17: *a) Examples of physical quantities whose structure is related to that of the probability $P(\boldsymbol{r}, \boldsymbol{r}')$ b) The basic building blocks used to calculate these quantities are the classical diffusion probability (the Diffuson), the correction related to phase coherence (the Cooperon), and the short range crossings. The symbol o represents a collision and the symbol $\times$ represents an arbitrary point in the medium.*